Quantification of Everest region glacier velocities between 1992 and 2002, using satellite radar interferometry and feature tracking

D.J. QUINCEY,[1] A. LUCKMAN,[2] D. BENN[3]

[1]*Centre for Glaciology, Institute of Geography and Earth Sciences, Aberystwyth University, Aberystwyth SY23 3DB, UK*
E-mail: djq@aber.ac.uk
[2]*School of the Environment and Society, Swansea University, Singleton Park, Swansea SA2 8PP, UK*
[3]*Department of Geology, The University Centre in Svalbard (UNIS), PO Box 156, NO-9171 Longyearbyen, Norway*

ABSTRACT. Many glacier snouts in the Himalaya are known to be stagnant and exhibiting low surface gradients, conditions that are conducive to the formation of glacial lakes impounded either by the terminal moraine or by the remnant glacier snout. In this study, we use interferometry and feature-tracking techniques to quantify the extent of stagnation in 20 glaciers across the Everest (Qomolangma; Sagarmatha) region, and subsequently we examine the relationship between local catchment topography and ice dynamics. The results show that only one of the studied glaciers, Kangshung Glacier, is dynamic across its entire surface, with flow rates greater than $40\,\mathrm{m\,a^{-1}}$ being recorded in high-elevation areas. Twelve other glaciers show some evidence of flow, but are generally characterized by long, stagnant tongues, indicating widespread recession and in situ decay. The remaining seven glaciers show no evidence of flow in any of the available datasets. Hypsometric data suggest that catchment topography plays an important role in controlling glacier flow regimes, with those fed by wide, high-altitude accumulation areas showing the most extensive active ice, and those originating at low elevations exhibiting large areas of stagnant ice. Surface profiles extracted from a SRTM digital elevation model indicate that stagnant snouts are characterized by very low ($<2°$) surface angles and that down-wasting is the prevalent ablation pattern in the study area.

1. INTRODUCTION

In high-altitude areas such as the central Himalaya, there is strong evidence connecting the recession of glacier ice to climatic adjustments associated with global warming (Oerlemans, 1994; Solomon and others, 2007). The relatively small mountain glaciers in such regions are 'summer accumulation types', dependent on monsoonal precipitation and cool summer temperatures for sustenance (Ageta and Higuchi, 1984). With temperatures having risen rapidly since the 1970s (Shrestha and others, 1999), precipitation has decreased (Qin and others, 2000) and snow precipitation has been partly replaced by rain on the lower elevations of the glaciers. The expected glaciological impact of such changes appears to vary depending on glacier catchment aspect, with north-flowing (predominantly clean-ice) glaciers responding by frontal recession, and south-flowing (debris-covered) glaciers wasting in situ (Kääb, 2005; Bolch and others, 2008b). The implications of continued Himalayan glacier recession are increased development of moraine-dammed lakes in the short term (Richardson and Reynolds, 2000; Benn and others, 2001) and shifts in the seasonal distribution of runoff in the longer term. It is therefore of utmost importance to be able to detect and monitor glacier recession in the region at the earliest opportunity.

On the debris-covered glaciers typical of large parts of the Himalaya, sustained periods of negative mass balance result in extensive down-wasting and stagnation of low-elevation glacier tongues, which frequently become de-coupled from the active upper glacier (e.g. Kadota and others, 2000). In such cases, frontal recession can be a poor indicator of glacier health, and multitemporal digital elevation datasets can be difficult and time-consuming to derive, at least at the required accuracy to be able to measure surface down-wasting trends over time periods less than a decade (Bolch and others, 2008b). Recent work, specific to the Everest (Qomolangma; Sagarmatha) region, has suggested that monitoring of flow rates can provide a useful proxy for glacier health where no other mass-balance information exists (Quincey and others, 2007). Further, this study found that local variations in glacier velocity and surface morphology between flow units control the precise location of lake growth based on single time-slices of velocity and information relating to glacier surface gradient. Subsequent to this, the methodological approaches available to quantify surface displacements over daily, monthly and annual time periods were detailed using time series of European Remote-sensing Satellite-1 and -2 (ERS-1/-2) synthetic aperture radar (SAR) data (Luckman and others, 2007) and optical satellite imagery (Bolch and others, 2008a; Scherler and others, 2008), albeit with limited glaciological interpretation.

The goal of the present study is to build on the findings of these previous contributions and widen the analysis both spatially and temporally, and to make a more detailed glaciological analysis of ice dynamics in the Himalayan region. Velocity data from throughout the 1990s and early 2000s are presented for 20 glaciers across the wider Everest region of Tibet (China) and Nepal, showing surface displacements from single-day (24 hour) to multi-annual timescales. The controlling parameters on glacier velocity patterns are explored through the use of topographic profiling and hypsometric analyses. The results are discussed within the context of wider Himalayan glacier recession and glacial lake development processes.
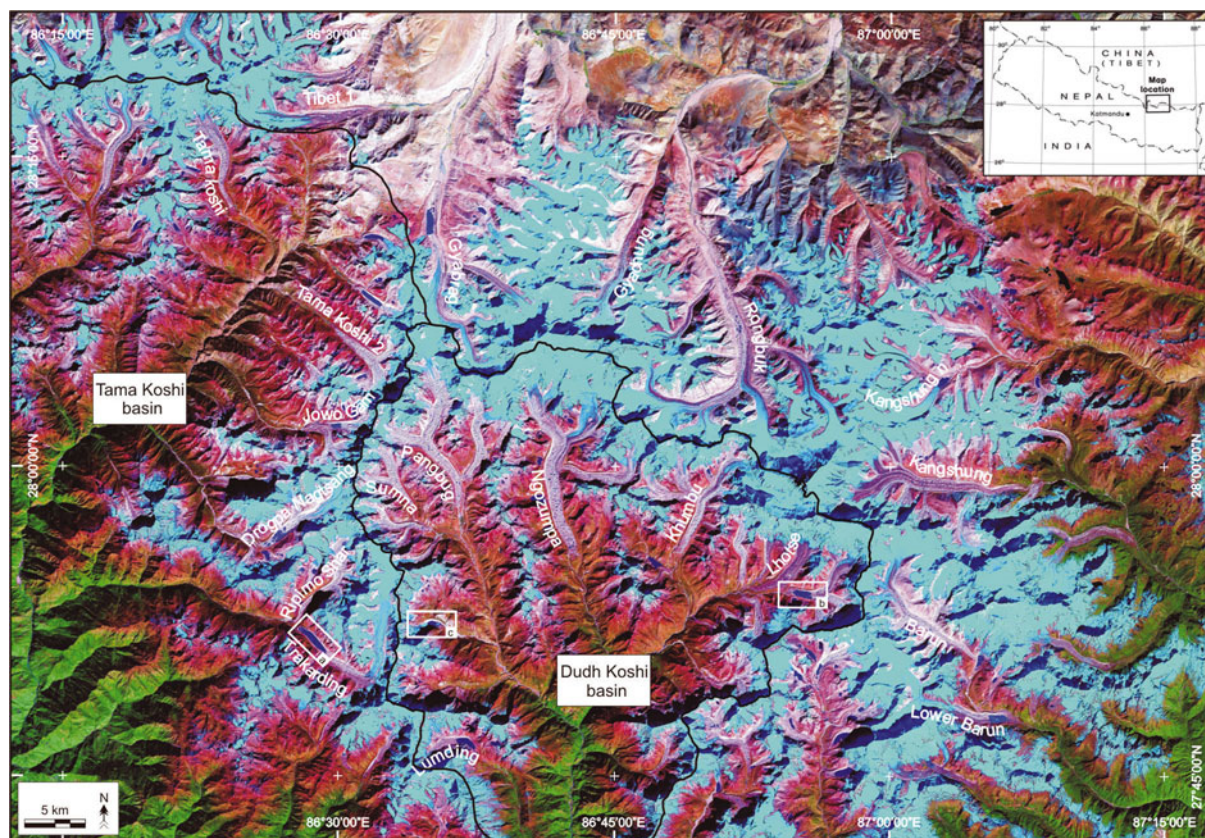
Fig. 1. Location of studied glaciers within the Dudh Koshi and Tama Koshi basins, Nepal and Tibet Himalaya. Note the existence of a number of large, moraine-impounded lakes (e.g. (a) Tsho Rolpa and (b) Imja Tsho), one of which catastrophically drained in 1985 ((c) Dig Tsho). Solid black lines delineate major watershed boundaries.

2. STUDY AREA, DATA SOURCES AND PROCESSING METHODS

The area studied surrounds the Everest massif of Nepal and Tibet (Fig. 1). The valley glaciers in this region are characterized by long, low-slope-angle, debris-covered tongues, which are bounded by massive moraine ridges and are fed by very high-altitude (6000–8000 m) clean-ice accumulation areas. Many of the glaciers in the region exhibit widespread surface ponding (Wessels and others, 2002) and exposed inner lateral moraine flanks, indicative of recent down-wasting and the early stages of glacial lake formation (Quincey and others, 2007). Indeed, a number of large lakes currently exist in the studied catchments (e.g. Imja Tsho (Watanabe and others, 1995); Tsho Rolpa (Reynolds, 1999)), and one major outburst flood has already occurred in recent decades (Dig Tsho, 4 August 1985), resulting in six fatalities, approximately US$1.5m worth of damage to a hydroelectric power station and the destruction of 30 houses and 14 bridges (S. Agrawala and others, http://www.oecd.org/dataoecd/6/51/19742202.pdf).

Within the catchments of the Dudh Koshi, the Tama Koshi and the immediate surrounding area, 20 glaciers were selected for study that exhibited a range of flow directions, surface characteristics and drainage patterns (Fig. 1). The area is covered by 16 ERS SAR frames acquired between 1992 and 2002 (Table 1). For the application of interferometry, tandem pair data (separated by 24 hours) were selected to maximize the possibility of maintaining coherence between image acquisitions. Images separated by time periods exceeding 1 year were also selected to maximize the

likelihood of deriving good-quality results from feature-tracking procedures, which require the identification of displaced features across two time-separated SAR images (Lucchitta and others, 1995). Shuttle Radar Topography Mission (SRTM) elevation data were acquired at a spatial resolution of 90 m (and resampled to 25 m) for the extraction of topographic surface profiles and hypsometric statistics. Image interpretation and topographic profile delineations were aided by a co-registered, orthorectified Landsat Enhanced Thematic Mapper Plus (ETM+) image (30 October 2000) at a spatial resolution of 30 m.

The techniques of interferometry and feature tracking were chosen because of their known complementarity in mountainous terrain (Luckman and others, 2007). On a temporal scale, interferometry provides information over daily (24 hour) periods (thus detecting, at times, transient velocities), and feature tracking provides annually averaged velocity fields (thereby removing any seasonal modulations in flow). In terms of spatial coverage, interferometry has been shown to perform best in clean-ice areas where coherence is well maintained (Quincey and others, 2007), whereas feature tracking works better over heavily debris-covered glacier tongues where distinct surface features are visible over long time periods (Kääb, 2005). The application of the two techniques together therefore provides multi-temporal velocity information over most glacierized areas. In the current study, processing for both interferometry and feature tracking followed well-developed and widely published procedures (e.g. Joughin and others, 1996; Strozzi and others, 2002), so only a brief outline of study-specific error analysis is given here.

Table 1. ERS-1/-2 SAR scenes covering the study area and used in the application of SRI and SRFT to derive glacier velocity data

	First image				Second image			Number of Julian days
Date	Orbit	Frame	A/D[*]	Date	Orbit	Frame	A/D[*]	
SRI								
29 Mar 1996	24606	0549	A	30 Mar 1996	04933	0549	A	1
12 Apr 1996	24799	3045	D	13 Apr 1996	05126	3045	D	1
3 May 1996	25107	0549	A	4 May 1996	05434	0549	A	1
17 May 1996	25300	3045	D	18 May 1996	05627	3045	D	1
SRFT								
2 Sep 1992	05918	3045	D	1 Dec 1993	12431	3045	D	455
1 Dec 1993	12431	3045	D	11 Aug 1995	21292	3045	D	618
11 Aug 1995	21292	3045	D	12 Apr 1996	24799	3045	D	245
4 May 1996	05434	0549	A	25 Sep 1998	37632	0549	A	874
18 May 1996	05627	3045	D	21 Jul 2001	32681	3045	D	1890
21 Jul 2001	32681	3045	D	14 Sep 2002	38693	3045	D	420

[*]Ascending/Descending.

In the absence of sufficiently coherent data for the 'double-differencing' approach (Gabriel and others, 1989), topographic phase was removed from computed interferograms through the use of precise orbit information (Scharroo and Visser, 1998) and SRTM data to yield line-of-sight (LOS) surface displacements. LOS displacements were subsequently converted to downslope rates using a locally smoothed SRTM digital elevation model (DEM), a process which can introduce two main sources of error to the final interferometric displacement results. First, in making the conversion from LOS to downslope velocities, any noise in the data is amplified, particularly where the look azimuth approaches an angle perpendicular to the flow azimuth. Therefore, in the current study, we mask out values within $20°$ of this perpendicular asymptote, to remove data with significant error from the presented results. Secondly, by using a DEM to re-project the LOS displacements, the accuracy of the final displacement data is partly dependent on any local topographic variability, resulting in some small areas of both artificially high and low velocity in the re-projected data. Therefore, in the current study we extracted the glacierized areas from the DEM and smoothed them prior to re-projection using a 50×50 pixel window to minimize the effect of local topography on the presented results. Some further noise is contributed by atmospheric and baseline error components (Mohr and others, 2003), which may add up to $\sim2.5\,\mathrm{cm\,d^{-1}}$ uncertainty. Combined, the atmospheric, baseline and DEM components contribute a maximum error of $\sim3\,\mathrm{cm\,d^{-1}}$ (equivalent to $\sim10\,\mathrm{m\,a^{-1}}$) to the 24 hour interferometric data.

Feature tracking was based on small (10×150 pixels) windows because of the abundance of surface features on the glacial and proglacial terrain. The centre pixel of each patch was assigned the displacement of the dominant feature within that patch, rather than an average displacement taken over the whole window. Consequently, a good degree of confidence can be placed in the derived data, even towards the margins of the glacier. Nevertheless, some errors in the feature-tracking data do result from changes in the surface features through time and space and geometric transformations of the data during the processing procedure. It is not possible to quantify exactly such errors, particularly those introduced by small mismatches of surface patterns that may have changed through time, but empirical measurements of displacement in known stationary areas suggest they are low. Further, in the current study, apparent matches on steeply sloping ($>20°$) terrain were filtered out and those in areas of layover and shadow were also rejected, leaving only the most robust of measurements. Therefore, the maximum error in the presented feature-tracking data is estimated to be of the order of $0.5\,\mathrm{cm\,d^{-1}}$ (equivalent to $\sim2\,\mathrm{m\,a^{-1}}$) for pairs separated by more than 1 year.

Full details of the processing methods used and a more comprehensive quantification of their associated errors are detailed elsewhere (Luckman and others, 2007).

3. APPLICATION TO GLACIERS IN NEPAL AND TIBET

Satellite radar interferometry (SRI) and feature-tracking (SRFT) procedures were applied to all available image pairs covering the selected glaciers across the Everest region. Glaciers were subsequently classified into three distinct groups (Table 2): type 1 – those glaciers showing displacement across the whole glacier surface; type 2 – those glaciers showing displacement, but only in upper areas of the debris-covered tongue or in the clean-ice zone; and type 3 – those glaciers showing no detectable activity anywhere across the glacier surface. This classification was made based on velocity fields extracted from both SRI and SRFT datasets.

3.1. Dynamics overview

Surface velocity fields derived by SRFT indicate extensive areas of stagnant ice on 19 of the 20 glaciers imaged. Seven of the studied glaciers showed no displacement. Only one glacier was classified as being of type 1, showing displacement across the whole of its surface in all of the image pairs.

The single type 1 glacier is Kangshung Glacier, which flows east from the massive (3350 m high) Kangshung face of Mount Everest. SRFT data indicate that the glacier is active even in its terminus region (Fig. 2a and b). From the terminus, measured surface displacements increase almost linearly with distance up-glacier (Fig. 3a). The velocity maximum of $\sim36\,\mathrm{m\,a^{-1}}$ is reached at a point 8 km from the terminus, beyond which the surface is obscured by layover so no further velocity data can be extracted.

Twelve of the studied glaciers are classified as being of type 2. They are mostly characterized by long, stagnant, debris-covered tongues, with flow only being detected in
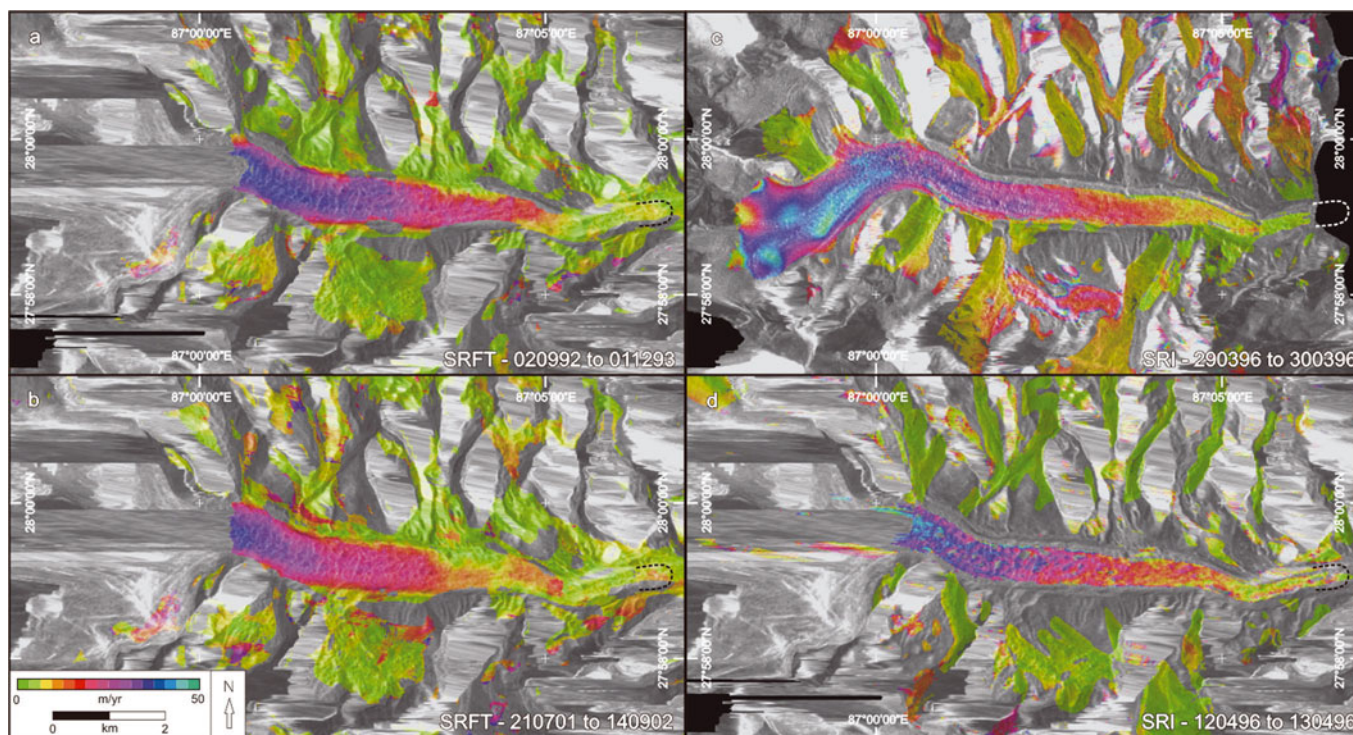
Fig. 2. Feature-tracking (a, b) and interferometric (c, d) data derived for the most active glacier within the studied area, Kangshung Glacier: (a) 2 September 1992 to 1 December 1993; (b) 21 July 2001 to 14 September 2002; (c) 29–30 March 1996; and (d) 12–13 April 1996. Dashed curves indicate approximate glacier terminus.

high-elevation areas. Of these, Ngozumpa Glacier stands out as being particularly active. SRFT data indicate that the lowermost 6.5 km of the tongue of Ngozumpa Glacier is almost stagnant (Fig. 4a), but that its western tributary remains dynamic. Flow increases rapidly up the western tributary, reaching the maximum recorded value of $\sim$45 m a^{-1}

within 5 km of the interpreted transition between active and stagnant ice (Fig. 3b). Several other glaciers show a similar trend. For example, the lowermost 3–4 km of Khumbu Glacier is shown to be stagnant, but from this point flow increases to a maximum of $\sim$20 m a^{-1} within a further 3 km (Figs 3c and 4b). The lowermost 3–4 km of Lhotse Glacier is

Table 2. Detected flows on Everest region glaciers and resulting classification of activity (types 1–3)

Glacier no.	Glacier name	Max detectable flow 1992/2002		Dynamics classification	Notes
		Clean ice m a^{-1}	Debris-covered ice m a^{-1}		
1	Kangshung	42	36	Type 1	Flow recorded across entire snout
2	Kangshung North	–	4	Type 3	Poor data coverage
3	Lhotse	48	28	Type 2	Very fast flow recorded directly beneath headwall
4	Ngozumpa	46	35	Type 2	No flow recorded within 6.5 km of terminus
5	Sumna	0	0	Type 3	No flow recorded on any part of glacier
6	Khumbu	20	16	Type 2	No flow recorded within 4 km of terminus
7	Rongbuk	19	11	Type 2	Low flow in clean-ice areas
8	Barun	4	6	Type 2	Flow only recorded in upper reaches
9	Lower Barun	3	0	Type 3	No flow recorded on any part of glacier
10	Tama Koshi	–	9	Type 2	No flow recorded within 4 km of terminus
11	Ripimo Shar	2	1	Type 3	No flow recorded on any part of glacier
12	Tama Koshi 2	–	11	Type 2	No flow recorded within 3 km of terminus
13	Jowo Gam	0	0	Type 3	No flow recorded on any part of glacier
14	Drogpa Nagtsang	24	6	Type 2	Low flow recorded in upper reaches
15	Tibetan (unnamed)	45	12	Type 2	Increasing flow from a point 5 km from the terminus
16	Gyabrag	5	12	Type 2	Patchy flow in debris-covered areas
17	Gyachung	4	12	Type 2	Uniform low flow across glacier surface
18	Lumding Tsho	–	6	Type 3	Flow recorded at calving ice front in 1992–93 dataset
19	Pangbug	0	0	Type 3	No flow recorded on any part of glacier
20	Trakarding	16	8	Type 2	Flow recorded beneath icefall in all datasets
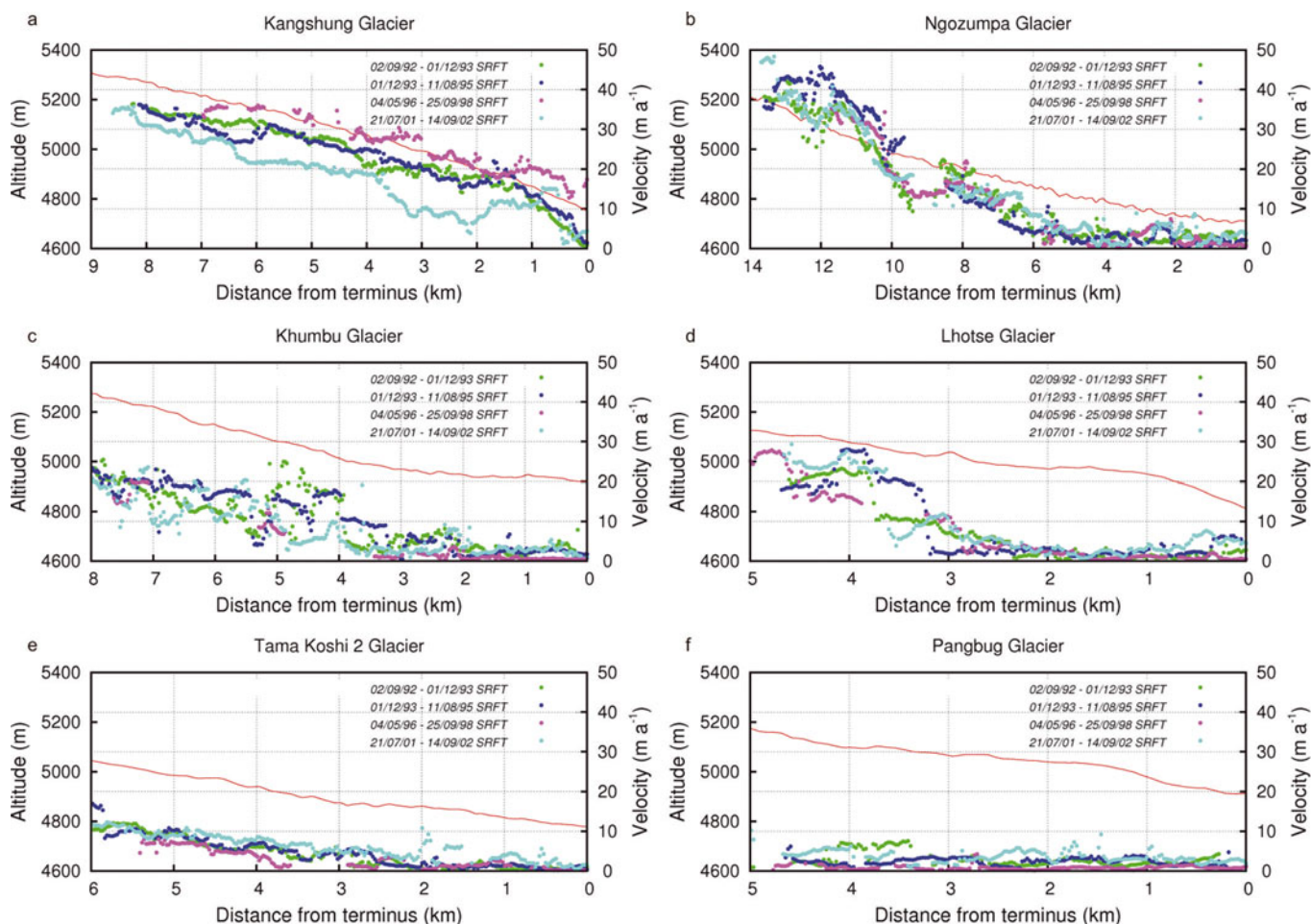
Fig. 3. Centre-line velocity and topography profiles for selected glaciers referred to in the text, derived from SRFT datasets: (a) Kanshung Glacier; (b) Ngozumpa Glacier; (c) Khumbu Glacier; (d) Lhotse Glacier; (e) Tama Koshi 2 Glacier; and (f) Pangbug Glacier. Topography is depicted by the thin red line. Dates are day/month/year.

also shown to be stagnant (Fig. 4c); here the velocity maximum of $\sim 25\,\mathrm{m\,a^{-1}}$ is reached within 1 km of the stagnant debris-covered tongue (Fig. 3d).

A small number of other type 2 glaciers appear to be characterized by very low flow, which is only evident in high-elevation areas. These glaciers are largely stagnant over the majority of their debris-covered area, but exhibit some flow in the transitional area between debris-covered and clean ice (Fig. 4d). Maximum recorded displacements reach approximately $10\,\mathrm{m\,a^{-1}}$ (Fig. 3e).

The remaining seven (type 3) glaciers show little commonality, other than their lack of detected surface displacement. They are spatially disparate and exhibit a range of catchment aspects. They appear not to be limited by size, with one of the longest glaciers in the imaged area (Pangbug Glacier; Figs 3f and 4e) and also one of the shortest glaciers in the imaged area (Jowo Gam Glacier) both falling within this group.

Twenty-four-hour displacement data derived by SRI are supportive of the patterns revealed over annual timescales by SRFT procedures. Kangshung Glacier stands out as being active across its entire debris-covered surface (Fig. 2c and d), and of the type 2 glaciers Ngozumpa Glacier is again shown to be very active on its western tributary (Fig. 5a). The local distribution of flow across the glacier surfaces is also similar; Kangshung Glacier is characterized by a still-active terminus with flow increasing gradually up-glacier to a maximum of

approximately $40\,\mathrm{m\,a^{-1}}$ (Fig. 6a), while Ngozumpa Glacier is characterized by a long (6.5 km), stagnant snout, with flow increasing very rapidly up to a maximum value of the order of $40–45\,\mathrm{m\,a^{-1}}$ (Fig. 6b), correlating well with the SRFT data.

The 24 hour SRI data also record flow in the upper parts of most of the other type 2 glaciers, supporting the spatial patterns identified by the feature-tracking results. For example, Lhotse Glacier again displays rapid flow in a localized area immediately beneath the steep accumulation zone (Fig. 5b). However, the SRI data are also successful in detecting zones of low-magnitude flow in transitional areas between clean- and debris-covered ice on several other glaciers (e.g. Drogpa Nagtsang, Rongbuk and an unnamed Tibetan glacier; Fig. 5c–e), patterns which were not evident in the SRFT data. Nevertheless, these glaciers are still characterized by large areas of stagnant ice towards their termini (Fig. 6d–f).

No surface displacement was detected on any of the type 3 glaciers previously identified by SRFT data.

3.2. Surface topography and glacier hypsometry

The surface topography of each glacier, as revealed by the profiles extracted from the SRTM DEM, demonstrates some correspondence between glacier activity and profile shape. The most dynamic of the glaciers within the study area, Kangshung Glacier, exhibits a distinctly convex topographic profile (Fig. 6a), whereas glaciers that are approaching
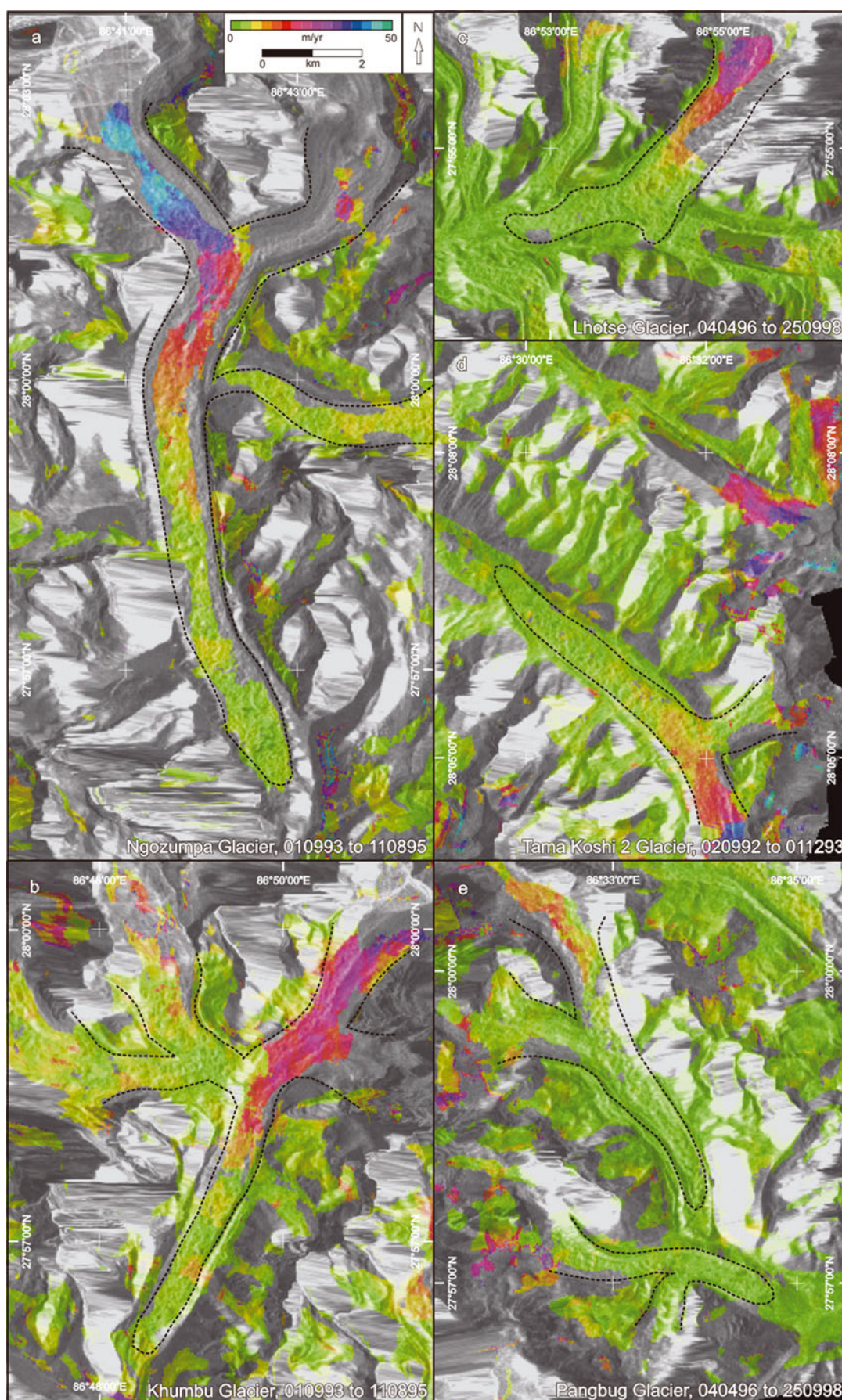
Fig. 4. Feature-tracking data derived for selected type 2 and type 3 glaciers: (a) Ngozumpa Glacier, displaying a long and stagnant tongue, but a very active western tributary; (b) Khumbu Glacier, which appears mostly stagnant for the lowermost 4 km of its tongue; (c) Lhotse Glacier, which is characterized by a very localized zone of fast flow immediately beneath its 3 km high accumulation headwall; (d) an unnamed glacier in the Tama Koshi catchment, which has very low flow in high-elevation areas; and (e) Pangbug Glacier, which is stagnant across its entire debris-covered area. Dashed curves delineate approximate glacier boundaries.
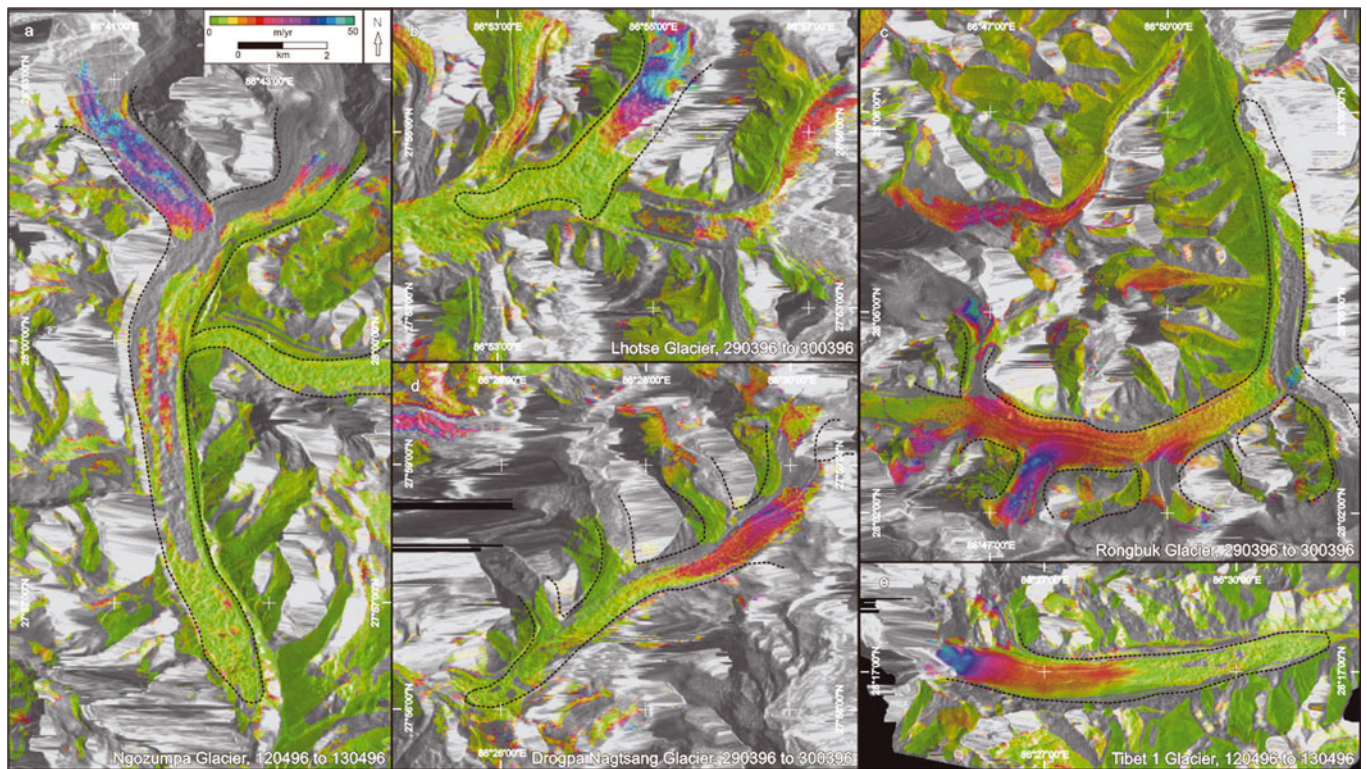
Fig. 5. Interferometric data derived for selected type 2 and type 3 glaciers: (a) Ngozumpa and (b) Lhotse Glaciers, showing displacement similar to that detected by SRFT (Fig. 4), and (c) Rongbuk Glacier, (d) Drogpa Nagtsang Glacier and (e) an unnamed Tibetan glacier, showing low flow in the transitional area between debris-covered and clean ice, patterns not evident in the SRFT data. Dashed curves delineate approximate glacier boundaries.

stagnation, or are already stagnant across their debris-covered tongues, are characterized by more linear topographic profiles (e.g. Ngozumpa and Rongbuk Glaciers; Fig. 6b and d). Some of the most stagnant glaciers exhibit very low-gradient (<2°) tongues (e.g. Drogpa Nagtsang Glacier; Fig. 6e), with elevation even increasing towards the terminus in places.

Hypsometric data also demonstrate a strong relationship with glacier type (Fig. 7); statistics relating area to elevation show that Kangshung Glacier (type 1) has a large accumulation area at very high altitude, whereas Pangbug Glacier (type 3) has a small accumulation area located at relatively low altitude. Both Kangshung and Khumbu Glaciers have large parts (~40%) of their total coverage at elevations exceeding 6000 m, whereas the less dynamic of the studied glaciers (Pangbug) has a much lower proportion (~20%) of its total coverage found above the 6000 m level. Further data relating the maximum elevation in a given catchment to the altitudinal range of the glacier support this trend (Fig. 8). A clear relationship exists between the elevation of glacier origin, its associated altitudinal range and the present-day ice dynamics, suggesting that the highest glaciers have historically reached furthest down-valley, and are currently those that remain the most active.

4. DISCUSSION

4.1. Spatial variability in glacier flow

In contrast to previous work in the eastern Himalaya (e.g. Kääb, 2005), glacier dynamics in the Everest region do not appear to be strongly linked with glacier catchment aspect, and all but one of the studied glaciers exhibit extensive areas

of stagnant ice. This reflects the contrasting distribution of clean-ice and debris-covered glaciers in the two regions. In the eastern Himalaya, north-facing glaciers are mainly clean, and have remained active during retreat, whereas glaciers on the higher-relief southern (Bhutan) slope of the Greater Himalaya are extensively debris-covered and are undergoing down-wasting and stagnation. In the Everest region, all large glaciers are debris-covered. Thick debris cover inhibits surface melting, resulting in inverted ablation gradients on the lower glaciers where debris cover is thickest (Benn and Lehmkuhl, 2000; Nicholson and Benn, 2006). During periods of negative mass balance, therefore, mass loss is less near the terminus than higher up the ablation zone, resulting in reduction of the glacier surface gradient, ice stagnation and surface down-wasting (Reynolds, 2000; Bolch and others, 2008b; Scherler and others, 2008).

The most active glacier, Kangshung Glacier, is distinct from other glaciers in the study area in two key ways. First, it descends from the eastern faces of Mount Everest (8848 m a.s.l.) and Baruntse (7220 m a.s.l.) into a number of large, high-altitude clean-ice plateaus, which then feed into the main glacier tongue. Topographic data suggest that upper parts of Kangshung Glacier are at sufficient height (see Fig. 7), and associated cool temperature, that the majority of precipitation falls as snow, resulting in a large annual accumulation budget. Secondly, because of the glacier's situation directly east of Mount Everest, it is likely to be preferentially fed, for the majority of the year, by wind-blown snow from the western face of the mountain. These two factors combined are interpreted to account for the exceptional dynamic regime of Kangshung Glacier compared to neighbouring ice masses.
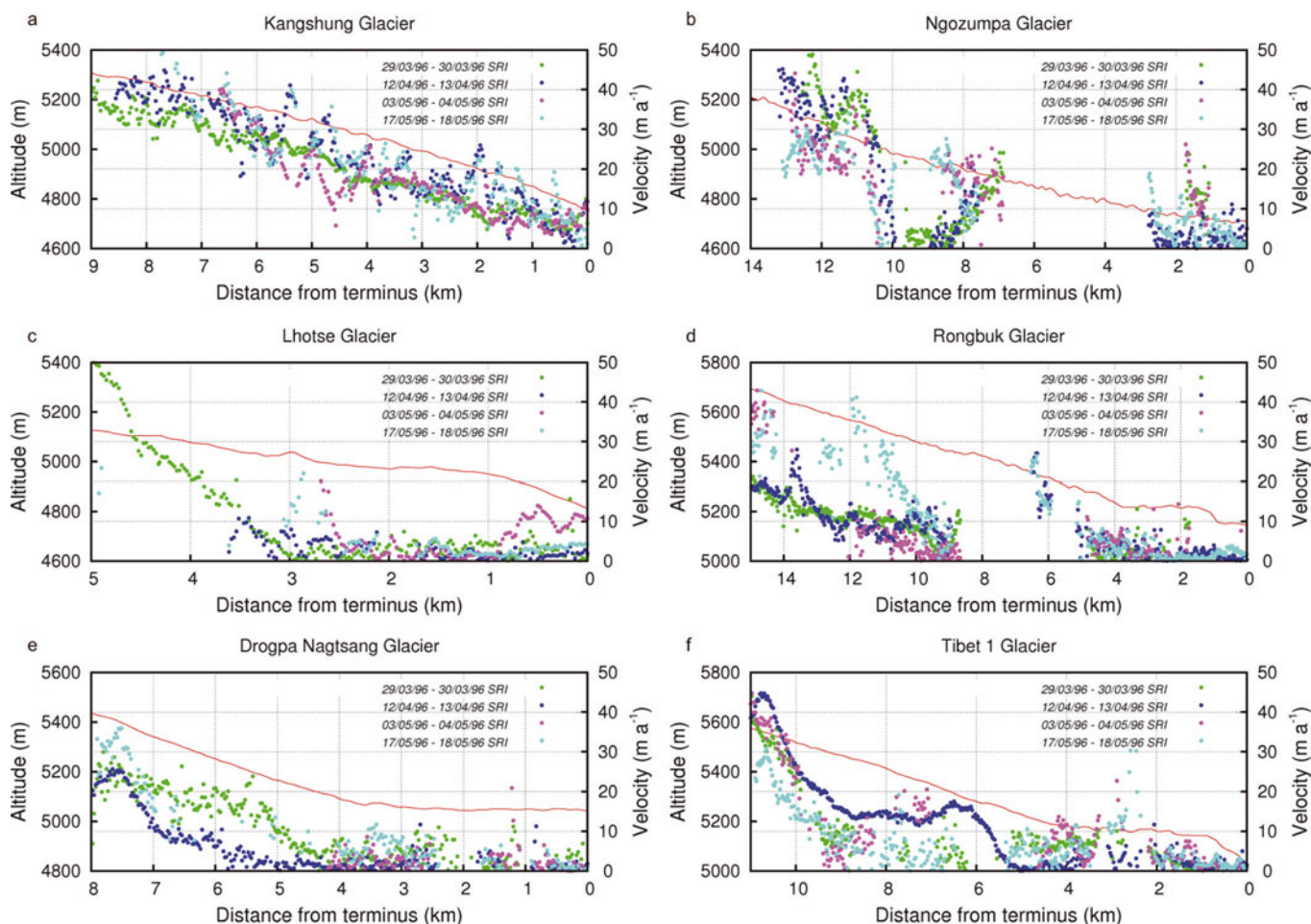
Fig. 6. Centre-line velocity and topography profiles for selected glaciers referred to in the text, derived from SRI datasets: (a) Kanshung Glacier; (b) Ngozumpa Glacier; (c) Lhotse Glacier; (d) Rongbuk Glacier; (e) Drogpa Nagtsang Glacier; and (f) Tibet 1 Glacier. Topography is depicted by thin red line. Dates are day/month/year.

The relatively high velocities measured on upper Ngozumpa Glacier also appear to reflect topographic controls. Its western tributary glacier originates from the southeast face of Cho Oyu (8201 m a.s.l.), the sixth highest mountain in the world, and descends into a relatively large and high-altitude accumulation area compared to neighbouring glaciers. In contrast, the near-stagnant tributary glacier to the northeast of the main trunk descends from a similar height, but the areal extent of the accumulation zone is much reduced in comparison.

These observations indicate that catchment topography plays an important role in controlling glacier velocity patterns in the region. Indeed, hypsometric data demonstrate that the single type 1 glacier, Kangshung Glacier, is fed by an unusually high and extensive accumulation area and that most of the ice is found at relatively high elevation (Fig. 7), factors which contribute to a dynamic glacier tongue even at the terminus. Type 2 glaciers (e.g. Khumbu Glacier) are also typically fed by very high rock headwalls, but with smaller areal extent and a more rapid descent into lower elevations when compared to Kangshung Glacier. Flow is therefore only maintained for several kilometres below the accumulation area. Type 3 glaciers (e.g. Pangbug Glacier) typically originate at relatively low altitude (<7500 m), with the greatest area of ice being found within the lowermost 1000 m (elevation) of the glacier.
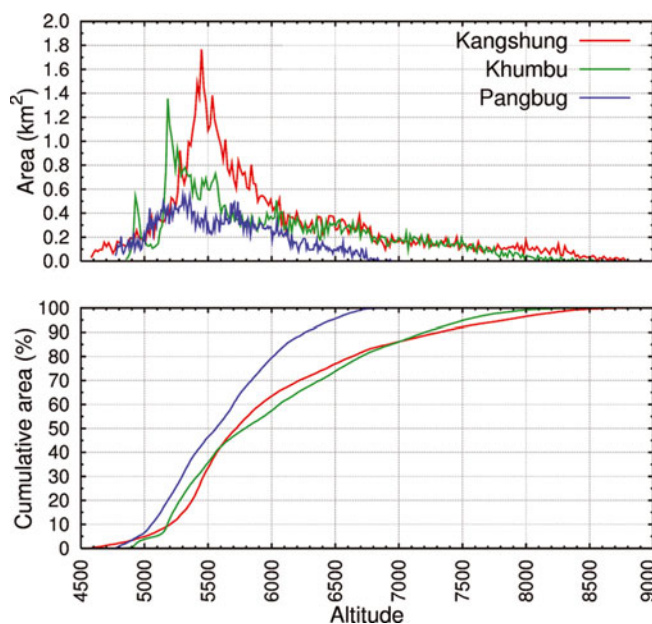
Fig. 7. Cumulative and standard hypsometric curves for one type 1 glacier (Kangshung Glacier), one type 2 glacier (Khumbu Glacier) and one type 3 glacier (Pangbug Glacier). Note the varying distribution of glacier area with altitude, which appears to be a control on glacier flow.
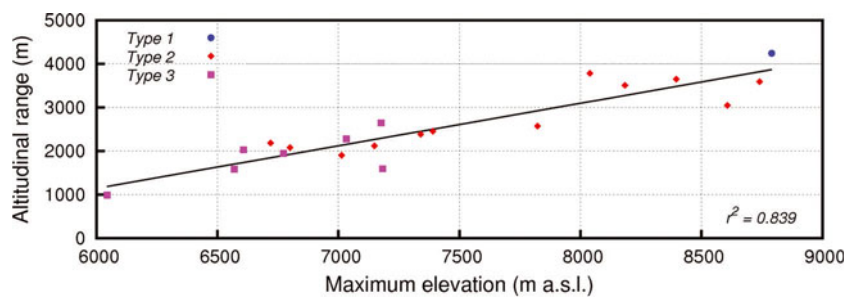
Fig. 8. Comparison of glacier altitudinal range with elevation of origin (maximum elevation). Elevation statistics were extracted from the SRTM DEM.

The relationship between ice dynamics and catchment topography is not clear-cut, however, as a number of other factors also play a significant role. For example, the accumulation characteristics of glaciers in the Everest region are strongly related to the availability of ice avalanche material in upper areas, making it very difficult to generalize even across sub-catchments feeding a single glacier. Nevertheless, data derived in the current study relating the elevation at the glacier origin to its altitudinal range do demonstrate that those glaciers forming at high elevations flow to comparatively low-elevation areas (Fig. 8), suggesting a strong topographic control on glacier length. The relationship between these two topographic variables and ice dynamics (during the observed period) is similarly strong, clearly demonstrating that the glaciers exhibiting the lowest velocities are those originating at low elevation. On such glaciers, recent climatic warming may have led to a reduction in accumulation as snowfall has been replaced, at least partly, by rain, which in turn is manifested in reduced flow rates and, ultimately, stagnation.

Many of the glaciers in the region have melt ponds on the low-gradient, stagnant part of their ablation areas (Wessels and others, 2002). The majority of these ponds are located well above the glacier terminus and are therefore likely to be 'perched lakes' which will drain if they connect with the englacial drainage system (Benn and others, 2001; Gulley and Benn, 2007). Although ephemeral, such lakes contribute disproportionately to glacier ablation, due to calving and subaqueous melting (Sakai and others, 1998; Benn and others, 2001), so pond formation on low-gradient glaciers will tend to amplify rates of downwasting (Sakai and others, 2000). When the down-wasting glacier surface reaches hydrological base level, determined by the elevation of the ice-cored terminal moraines, lake expansion can continue unchecked until the moraine dam is incised or fails. Large areas of stagnant ice in the region, as detected in this study, therefore imply further lake development and an increased risk of glacier lake outburst floods in the coming decades.

4.2. Topographic profile shape as a proxy for glacier health

Topographic data collected from the 20 glaciers in this study suggest that the shape of the centre-line profile may be used as an indicator of glacier health. Our data suggest that dynamic Himalayan glaciers (e.g. Kangshung Glacier) can be characterized by a convex topographic profile indicating a large throughput of mass to the debris-covered tongue from higher-elevation areas. As the glacier stagnates, thick debris towards the glacier terminus insulates the ice from ablation (Nakawo and others, 1999), whereas thinner debris further up-glacier cannot inhibit surface melting as effectively, resulting in higher ablation rates (Benn and Lehmkuhl, 2000). Therefore, in times of negative mass balance, mass loss is often greatest at a point several kilometres up-glacier of the terminus (Kadota and others, 2000), thus gradually reducing the overall glacier surface gradient. The surface profile of the glacier first flattens out, and ultimately adopts a concave form (e.g. Ngozumpa Glacier; Fig. 6b), with the lower parts of the glacier tongue approaching the horizontal (e.g. Drogpa Nagtsang Glacier; Fig. 6e). In extreme cases, a reverse gradient may even be observed. These analyses suggest that with freely available SRTM DEM data and Landsat Thematic Mapper (TM)/ETM+ imagery, limited assessments of glacier health, low surface angles and, therefore, potential lake development sites are possible even in areas where no other available data exist.

4.3. Comparisons with published data

There have been relatively few other studies recording historical glacier velocities in the region; indeed, only Khumbu Glacier appears to have been the subject of published records of flow preceding 1990. Those data that are available with which to compare our SRI and SRFT results indicate that Khumbu Glacier has experienced some slowdown since previously published work. Flow rates of around $30 \, \text{m} \, \text{a}^{-1}$ were recorded at Gorak Shep on Khumbu Glacier in the late 1960s (Nakawo and others, 1999). For the same point in more contemporary imagery (1990s–current study), both the SRI and SRFT velocity data suggest ice movement was approximately 20% of the 1960s value (Luckman and others, 2007). The most recent data available, generated from optical feature tracking during the early 2000s, generally support these findings, suggesting that the modern-day ice movement at Gorak Shep is of the order of 30–40% of the 1960s value (Bolch and others, 2008a; Scherler and others, 2008), slightly higher than those data derived in the current study.

Contemporary measurement of south-flowing debris-covered glaciers in the Bhutan Himalaya reveals velocities of $20–50 \, \text{m} \, \text{a}^{-1}$, greatly in excess of those detected in the Everest region (Kääb, 2005). Even greater differences are shown for northern-flowing predominantly clean-ice glaciers: Kääb (2005) recorded flows of up to $100–200 \, \text{m} \, \text{a}^{-1}$, compared to flows of around $20 \, \text{m} \, \text{a}^{-1}$ on the more heavily debris-covered surfaces in the Everest region. Such results indicate that widespread areas of stagnant ice, as detected here in the Everest region, may not be representative of a wider Himalayan trend.

5. CONCLUSIONS

SRI and SRFT have been successfully employed to measure glacier velocities across the Everest region of Nepal and Tibet. Little spatial variability in flow was detected, with the exception of the Kangshung and Ngozumpa tributary glaciers, which both showed annual displacements exceeding any other glacier within the study area. Nineteen of the twenty studied glaciers were found to be stagnant or approaching stagnation across large parts of their debris-covered areas. Hypsometric data extracted from the SRTM DEM suggested that there is a strong topographic control on glacier flow in the region, with those glaciers being fed by the highest and widest accumulation areas reaching furthest down-valley and showing the greatest surface displacements over the observed period. The use of SRTM elevation data for extracting topographic profiles was also demonstrated, and the results indicated that the surface elevation profile of the glacier may be used as a proxy for glacier health in the absence of other supporting data.

These results suggest that glaciers in the Everest region are in poor health, characterized by low flow at high elevations, and long, stagnant, debris-covered tongues at lower elevations. The short-term implication (i.e. next 10 years) of stagnant and near-stagnant glacier ice melting at high altitude is for increased development of large-scale glacial lakes, particularly on debris-covered glaciers where in situ decay promotes meltwater ponding and lake growth, behind either remnant glacier ice or the terminal moraine. Longer-term, there is likely to be a knock-on effect for water resources, although the exact temporal and spatial shifts in runoff distribution remain poorly understood. It is therefore imperative that such glaciers are regularly monitored using techniques such as those demonstrated here, both in the Everest region and elsewhere, and that further efforts are made to understand the locally specific response of Himalayan glaciers to sustained climatic forcing, so that more accurate predictions of changes to seasonal and annual runoff regimes can be made.

REFERENCES

Ageta, Y. and K. Higuchi. 1984. Estimation of mass balance components of a summer-accumulation type glacier in the Nepal Himalaya. *Geogr. Ann.,* **66A**(3), 249–255.

Benn, D.I. and F. Lehmkuhl. 2000. Mass balance and equilibrium-line altitudes of glaciers in high mountain environments. *Quat. Int.,* **65/66**, 15–29.

Benn, D.I., S. Wiseman and K.A. Hands. 2001. Growth and drainage of supraglacial lakes on the debris-mantled Ngozumpa Glacier, Khumbu Himal, Nepal. *J. Glaciol.,* **47**(159), 626–638.

Bolch, T., M.F. Buchroithner, J. Peters, M. Baessler and S. Bajracharya. 2008a. Identification of glacier motion and potentially dangerous glacial lakes in the Mt. Everest region/Nepal using spaceborne imagery. *Natur. Hazards Earth Syst. Sci. (NHESS),* **8**(6), 1329–1340.

Bolch, T., M. Buchroithner, T. Pieczonka and A. Kunert. 2008b. Planimetric and volumetric glacier changes in the Khumbu Himal, Nepal, since 1962 using Corona, Landsat TM and ASTER data. *J. Glaciol.,* **54**(187), 592–600.

Gabriel, A.K., R.M. Goldstein and H.A. Zebker. 1989. Mapping small elevation changes over large areas: differential radar interferometry. *J. Geophys. Res.,* **94**(B7), 9183–9191.

Gulley, J. and D.I. Benn. 2007. Structural control of englacial drainage systems in Himalayan debris-covered glaciers. *J. Glaciol.,* **53**(182), 399–412.

Joughin, I., R. Kwok and M. Fahnestock. 1996. Estimation of ice-sheet motion using satellite radar interferometry, *J. Glaciol.,* **42**(142), 564–575.

Kääb, A. 2005. Combination of SRTM3 and repeat ASTER data for deriving alpine glacier flow velocities in the Bhutan Himalaya. *Remote Sens. Environ.,* **94**(4), 463–474.

Kadota, T., K. Seko, T. Aoki, S. Iwata and S. Yamaguchi. 2000. Shrinkage of the Khumbu Glacier, east Nepal from 1978 to 1995. *IAHS Publ.* 264 (Symposium at Seattle 2000 – *Debris-Covered Glaciers*), 235–243.

Lucchitta, B.K., C.E. Rosanova and K.F. Mullins. 1995. Velocities of Pine Island Glacier, West Antarctica, from ERS-1 SAR images. *Ann. Glaciol.,* **21**, 277–283.

Luckman, A., D.J. Quincey and S. Bevan. 2007. The potential of satellite radar interferometry and feature tracking for monitoring flow rates of Himalayan glaciers. *Remote Sens. Environ.,* **111**(2–3), 172–181.

Mohr, J.J., N. Reeh and S.N. Madsen. 2003. Accuracy of three-dimensional glacier surface velocities derived from radar interferometry and ice-sounding radar measurements. *J. Glaciol.,* **49**(165), 210–222.

Nakawo, M., H. Yabuki and A. Sakai. 1999. Characteristics of Khumbu Glacier, Nepal Himalaya: recent changes in the debris-covered area. *Ann. Glaciol.,* **28**, 118–122.

Nicholson, L. and D.I. Benn. 2006. Calculating ice melt beneath a debris layer using meteorological data. *J. Glaciol.,* **52**(178), 463–470.

Oerlemans, J. 1994. Quantifying global warming from the retreat of glaciers. *Science,* **264**(5156), 243–245.

Qin, D. *and 9 others.* 2000. Evidence for recent climate change from ice cores in the central Himalaya. *Ann. Glaciol.,* **31**, 153–158.

Quincey, D.J. *and 6 others.* 2007. Early recognition of glacial lake hazards in the Himalaya using remote sensing datasets. *Global Planet. Change,* **56**(1–2), 137–152.

Reynolds, J.M. 1999. Glacial hazard assessment at Tsho Rolpa, Rolwaling, central Nepal. *Q. J. Eng. Geol.,* **32**(3), 209–214.

Reynolds, J.M. 2000. On the formation of supraglacial lakes on debris-covered glaciers. *IAHS Publ.* 264 (Symposium at Seattle 2000 – *Debris-Covered Glaciers*), 153–161.

Richardson, S.D. and J.M. Reynolds. 2000. An overview of glacial hazards in the Himalayas. *Quat. Int.,* **65/66**, 31–47.

Sakai, A., M. Nakawo and K. Fujita. 1998. Melt rate of ice cliffs on the Lirung Glacier, Nepal Himalayas, 1996. *Bull. Glacier Res.* 16, 57–66.

Sakai, A., N. Takeuchi, K. Fujita and M. Nakawo. 2000. Role of supraglacial ponds in the ablation process of a debris-covered glacier in the Nepal. *IAHS Publ.* 264 (Symposium at Seattle 2000 – *Debris-Covered Glaciers*), 119–130.

Scharroo, R. and P. Visser. 1998. Precise orbit determination and gravity field improvement for the ERS satellites. *J. Geophys. Res.,* **103**(C4), 8113–8127.

Scherler, D., S. Leprince and M.R. Strecker. 2008. Glacier-surface velocities in alpine terrain from optical satellite imagery – accuracy improvement and quality assessment. *Remote Sens. Environ.,* **112**(10), 3806–3819.

Shrestha, A.B., C.P. Wake, P.A. Mayewski and J.E. Dibb. 1999. Maximum temperature trends in the Himalaya and its vicinity:

an analysis based on temperature records from Nepal for the period 1971–1994. *J. Climate,* **12**(9), 2775–2786.

Solomon, S. *and 7 others*, eds. 2007. *Climate change 2007: the physical science basis. Contribution of Working Group I to the Fourth Assessment Report of the Intergovernmental Panel on Climate Change.* Cambridge, etc., Cambridge University Press.

Strozzi, T., A. Luckman, T. Murray, U. Wegmuller and C.L. Werner. 2002. Glacier motion estimation using satellite-radar offset-tracking procedures. *IEEE Trans. Geosci. Remote Sens.,* **40**(11), 2834–2391.

Watanabe, T., S. Kameyama and T. Sato. 1995. Imja Glacier dead-ice melt rates and changes in a supra-glacial lake, 1989–1994, Khumbu Himal, Nepal: danger of lake drainage. *Mt. Res. Dev.,* **15**(4), 292–300.

Wessels, R.L., J.S. Kargel and H.H. Kieffer. 2002. ASTER measurement of supraglacial lakes in the Mount Everest region of the Himalaya. *Ann. Glaciol.,* **34**, 399–408.

MS received 17 July 2008 and accepted in revised form 8 January 2009